IOPscience iopscience.iop.org

Home Search Collections Journals About Contact us My IOPscience

The effect of argon on the structure of amorphous SiBCN materials: an experimental and *ab initio* study

This article has been downloaded from IOPscience. Please scroll down to see the full text article.

2006 J. Phys.: Condens. Matter 18 2337

(http://iopscience.iop.org/0953-8984/18/7/019)

View the table of contents for this issue, or go to the journal homepage for more

Download details:
IP Address: 129.252.86.83
The article was downloaded on 28/05/2010 at 08:59

Please note that terms and conditions apply.

INSTITUTE OF PHYSICS PUBLISHING JOURNAL OF PHYSICS: CONDENSED MATTER
J. Phys.: Condens. Matter **18** (2006) 2337–2348 doi:10.1088/0953-8984/18/7/019

The effect of argon on the structure of amorphous SiBCN materials: an experimental and *ab initio* study

J Houska[1,2], **O Warschkow**[1], **M M M Bilek**[1], **D R McKenzie**[1], **J Vlcek**[2] **and S Potocky**[2]

[1] School of Physics, The University of Sydney, NSW 2006, Australia
[2] Department of Physics, University of West Bohemia, Univerzitni 22, 30614 Plzen, Czech Republic

E-mail: jhouska@kfy.zcu.cz

Received 30 June 2005
Published 3 February 2006
Online at stacks.iop.org/JPhysCM/18/2337

Abstract
It has previously been noted that the implantation of argon atoms into amorphous SiBCN materials (prepared by magnetron sputtering in various N_2 + Ar mixtures) leads to variations in a number of material properties; for example an increase in compressive stress. Little is known about the mechanism by which Ar incorporation affects structural and mechanical properties of these materials. Here, we report *ab initio* molecular dynamics simulations of amorphous SiBCN materials. Using liquid-quench simulations, we investigate how the presence of Ar atoms in the sample affects the liquid quench and the final structure of the material. In the absence of Ar, we find that the final structures are homogenous. The presence of Ar, however, leads to the formation of Si-enriched regions in the vicinity of implanted Ar atoms. This result provides new insight into the role of implanted Ar in the formation of structures in amorphous SiBCN materials. It can also explain the ability of Si to relieve stress generated by these implanted Ar atoms.

1. Introduction

In recent years, amorphous SiBCN ceramics prepared by precursor pyrolysis at elevated temperatures [1–11] or CVD [12–14] have attracted great interest due to a number of exceptional material properties. Depending on the elemental composition, materials have been reported that feature one or more of high thermal stability [2–10], oxidation resistance [3, 10, 14, 15], hardness [15], creep resistance at elevated temperatures [2, 11], transparency and low stress [13, 15] and low thermal expansion coefficient [5]. With these properties, SiBCN materials have many potential applications in coating technologies [12, 14], microelectronics [1, 12] or the production of thermally stable fibres for composites [9].

© 2006 IOP Publishing Ltd Printed in the UK

In our recent work [15], we reported the preparation of SiBCN materials by magnetron sputtering. The advantages of the sputtering technique include its compatibility with semiconductor processing technologies, ease of scale-up, low deposition temperatures and reduced hydrogen content in comparison with materials prepared by chemical methods such as polymer pyrolysis or chemical vapour deposition. Since sputtering is typically performed in an Ar-containing atmosphere, materials prepared with this method are found to contain small amounts of implanted Ar atoms. These atoms arise from the impact of energetic Ar atoms or ions from the discharge or reflection from the sputtering target [16]. Implantation of Ar has been correlated with the presence of compressive stress in the films [17, 18].

In this work, we report experimental results which suggest that compressive stress created by implanted Ar atoms is more effectively relieved in SiBCN films with high Si content. First-principles simulations are performed to understand these observations at an atomistic level. We discuss the structural effects of Ar on the network and how high Si content may help relieve compressive stress.

2. Methodology

2.1. Ab initio simulations

The simulations reported in this work use a first-principles molecular dynamics model as implemented in the CPMD software [19]. The density functional theory (DFT) equations are solved in the generalized gradient approximation (GGA, BLYP functional [20, 21]) using a basis of plane waves with a cut-off of 60 Ryd. Core electrons were represented using Goedecker-type pseudopotentials [22] for Si, B, C and N and by a Troullier–Martins pseudopotential [23] for Ar. The accuracy of this method as well as the convergence of calculated properties with respect to plane-wave cut-off has been confirmed previously [24] for Si, B, C and N. The *ab initio* molecular dynamics (MD) method integrates the classical equations of motion for the nuclei and thereby provides insights into the time evolution of the system. All MD runs were performed using a time step of 0.073 fs and the fictitious electron mass (required for the classical integration of the electronic degrees of freedom) was set to 200 m_e.

Because the internal network structure and material properties of amorphous materials are intensively dependent on the formation conditions (the cooling rate of the liquid quench and the ordering processes that occur while the material solidifies from the melt), meaningful computer simulations of this type of material must focus on the formation process. In our simulation work, we try to capture this formation process using a liquid-quench algorithm. This approach has been used successfully in the prediction of the local atomic structure and material characteristics of a variety of amorphous materials, such as C [25–27], H:C [28], C doped by N [29], (B)(Al)N [30] or H:SiC [31].

In this algorithm it is assumed that the primary impact of energetic ions creates a *thermal spike*, that is, a localized region of high temperature, which is followed by exponential cooling to the solid state. Important in this is that the cooling rates, which can be estimated from the thermal diffusivity and the thermal spike radius [25], are short enough for *ab initio* MD simulations to be feasible.

In the liquid-quench algorithm, we mix the material by melting in order to remove memory of the initial configuration, followed by exponential cooling with a selected cooling rate down to the deposition temperature, followed in turn by equilibration of the material at the deposition temperature until a stable structure is established. In this protocol, ion bombardment at different energies is simulated by changes in the cooling rate.

MD simulation of N-containing materials such as SiBCN may lead to the formation of N_2 molecules in the simulation cell. We expect that every N_2 molecule formed during the synthesis escapes from the deposited material since the thermal spike in which the molecules are formed is always close to the material surface. The absence of N_2 molecules was experimentally confirmed by thermogravimetric analysis [15], which revealed no mass loss (indicative of N_2 outgassing) up to 1300 °C. As the molecules are likely to diffuse out of the real material, our simulations involve an ad hoc N_2 removal procedure. As we have shown in our recent publication [24], the formation of N_2 molecules is most intensive in the temperature window of 3000–6000 K. In order to compensate for N atom loss and still achieve a desired N content in the quenched material, the liquid-quench simulation has to be started with sufficient N excess. Our calculations were started with 100 atoms of experimental composition and up to 32 excess N atoms in a cell of experimental atomic density. In a separate publication we discuss our detailed simulation protocol that accounts for N_2 formation and diffusion out of the structure and still yields a material of desired N content [32]. This structure is then exponentially cooled from 3000 K to the experimental substrate temperature of 650 K. Temperature control was achieved by velocity scaling of ions when the simulation and target temperatures differed by more than 10%. By adjusting the cooling time in this phase of the simulation, we can simulate the effect of different ion bombardment energies as discussed in [25]. The cooling run was followed by an equilibration run (1 ps MD at 650 K, Nose–Hoover thermostat) in order to recover thermal equilibrium. All properties of interest were computed in a subsequent MD run (production run) of at least 0.5 ps at 650 K.

2.2. Film preparation and characterization

SiBCN films were deposited on Si(100) substrates by reactive dc magnetron co-sputtering of Si, B and C in N–Ar gas mixtures using a composite Si/B/C target. In this setup, the elemental composition and structure of the films are determined by the composition of the erosion target area, the gas mixture, the temperature of the substrate and the rf induced negative substrate bias voltage (U_b) which controls the energy of ion bombardment. In order to examine compressive stress as a function of Si and Ar content, a set of 30 samples was prepared by combining six different target compositions with five different deposition conditions (gas composition, substrate bias and temperature). The six target compositions were $Si_x(B_4C)_{100-x}$ with $x = 0, 5, 20, 40, 60, 75$. The five depositions conditions were: (1) 50% Ar + 50% N_2 gas mixture and substrate temperature of 650 K with $U_b = -100$ V; (2) the same with $U_b = -500$ V; (3) 75% Ar + 25% N_2 gas mixture with $U_b = -100$ V and substrate temperature of 1000 K; (4) the same with substrate temperature of below 500 K (no ohmic heating); and (5) discharge gas of 100% Ar with $U_b = -100$ V and substrate temperature of 650 K. Compressive stresses and elemental compositions were measured for all 30 samples. We note that the elemental analysis confirmed that the percentage of Si in the films increases with the ratio of Si in the sputtered target. Full details of our experimental setup can be found in [15].

The film thickness and compressive stress (calculated using Stoney's equation [33]) were measured using profilometry. The elemental concentrations of Si, B, C, N and Ar in the films were determined by Rutherford back-scattering spectroscopy (RBS). In selected cases, the B content was determined using neutron depth profiling. The atomic density of the films was determined using the number of film atoms per cm^2 as measured by RBS divided by the film thickness as given by profilometry. Thicknesses of deposited films were 1–7 μm at surface atomic densities around 1.0×10^{19} atoms cm^{-2} per 1 μm of film thickness. This leads to volume atomic densities (used in the simulations) of around 100 atoms nm^{-3}.

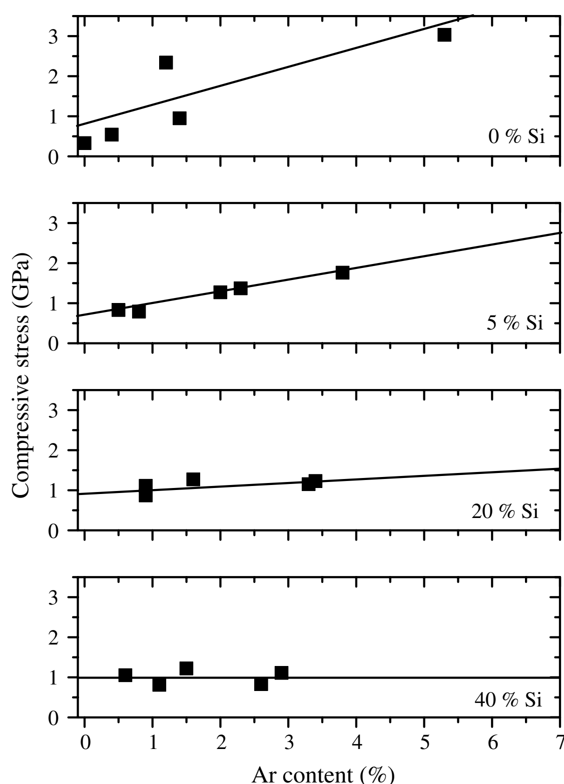

Figure 1. Experimental compressive stresses in SiBCN films as a function Ar and Si content. The lines are fits from linear regression. The figure shows that the linear dependence of stress and Ar content decreases with an increase in the Si content. Samples are prepared as described in the text. Not shown are the results for samples with 60 and 75% Si content in the B_4C target, which, like the 40% samples, did not exhibit any correlation of stress and Ar content.

Our simulations in this paper focus on samples of composition $Si_{32}B_{10}C_6N_{52}$ (deposited previously with various U_b between 0 and −500 V) and $Si_{32}B_{10}C_6N_{52}Ar_6$ ($U_b = -500$ V). The stronger Ar bombardment (discharge mixture Ar/N_2 = 3:1 instead of 1:1) increased both the content of implanted Ar in the second sample and its atomic density. A cooling time of 500 fs was used to simulate materials deposited with $U_b = -500$ V, while shorter cooling times were used to simulate the effect of lower $|U_b|$. Although all deposited samples contain small amounts of hydrogen, this was not considered in the simulations.

3. Results

3.1. Experimental results

Figure 1 shows the compressive stress measured in the 30 SiBCN samples as a function of Si and Ar content. The results show that for samples with low Si content, there exists a linear dependence between the amount of implanted Ar and the compressive stress in the films. For the samples with higher Si content, the correlation between Ar content and compressive stress is less clear in the 20% Si targets and there is no observable dependence in the 40, 60 and 75% Si targets. Collectively, the data show that an increase in Si content results in a decrease in

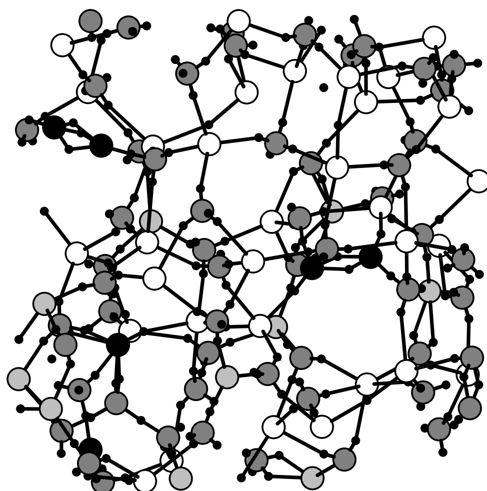

Figure 2. Snapshot from the end of the liquid-quench simulation of a SiBCN material of composition $Si_{32}B_{10}C_6N_{52}$ with no Ar atoms in the structure. Large black circles are C, medium grey are N, light grey are B, white circles correspond to Si, and the small black dots represent Wannier function centres (WFCs).

the dependence of compressive stress on Ar content. These results suggest that implanted Ar is a source of compressive stress in SiBCN films with low Si content, while in high Si content samples, stress generation through implanted Ar appears to be inhibited.

3.2. Computer simulation results

The objectives of our simulations are to understand the experimental results shown above. In particular we would like to understand by what mechanism high Si content leads to a more efficient stress release when Ar is present.

We first discuss our simulations of a sample of composition $Si_{32}B_{10}C_6N_{52}$ where our initial objective is to demonstrate that this composition prefers a homogeneous distribution of atoms in the network; i.e. this material does not segregate into locally distinct regions. Because our simulations are run in relatively small unit cells, a demonstration of homogeneity in a network is not straightforward. This is because we have to distinguish between genuine and coincidental segregation; the latter describes the situation that the initial distribution of atoms contains random inhomogeneities.

Full liquid-quench simulations were performed for this composition with exponential cooling times of 100 and 500 fs (corresponding to bias voltages U_b of −100 and −500 V, respectively). A typical snapshot of a structure obtained from these simulations is shown in figure 2. In the upper part of the figure, we can see a region of SiN_x containing no B and C atoms.

In order to quantify the segregation we introduce two criteria. Since we have more that 50% N in our compositions, likely binary regions are SiN_x or BN_x or CN_x. Our first criterion to measure the presence of such regions is the percentage of N atoms bonded only to one of Si, B or C. The number of bonds between atoms of the same kind is a second criterion, which detects the existence of elemental regions (such as pure Si or C networks).

Figure 3 shows these criteria applied to structures prior to cooling and after cooling runs of 50, 100, 250 and 500 fs. The data show a continuous reduction of both segregation criteria;

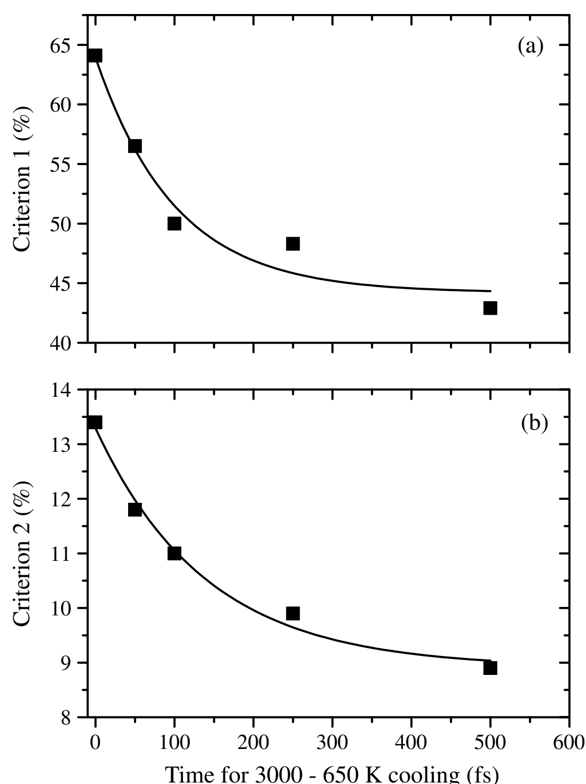

Figure 3. Dependence of segregation in quenched structures of composition $Si_{32}B_{10}C_6N_{52}$ on the time taken to quench from 3000 to 650 K. Segregation was measured using two criteria. Criterion 1 shown in (a) is the percentage of N atoms bonded to only one atom type (B, C, or Si) other than N. Criterion 2 shown in (b) is the percentage of chemical bonds between atoms of the same type. For both criteria, higher values are indicative of a less homogenous structure. The 0 fs data point measures segregation in the molten structure prior to cooling. Subsequent data points characterize the structures just after cooling to 650 K.

thus, there is a general increase in structural homogeneity with increased cooling time. We conclude that the initial SiN_x region detected in the structure in figure 2 is the result of random clustering in the melt.

This result suggests that the $Si_{32}B_{10}C_6N_{52}$ composition has a thermodynamic preference for a maximally homogenous structure. Long cooling times occur for impacts of high energy (high $|U_b|$ such as 500 V), for which we expect materials of homogeneous structure. In materials deposited with small $|U_b|$ such as 100 V some segregated regions such as SiN_x may survive.

We now examine the effect of implanted Ar on the SiBCN network. For this purpose six additional Ar atoms were added into the network to form the composition $Si_{32}B_{10}C_6N_{52}Ar_6$ and simulations were performed with a cooling time of 500 fs. A typical structure from the simulation is shown in figure 4, showing the distribution of Ar atoms. The Ar atoms are not bonded into the network (note how the WFCs associated with Ar are non-bonding). Five of the six Ar atoms lie close together. The non-bonding character of the Ar creates 'cavities' around them.

In order to determine the effect of implanted Ar atoms on structural homogeneity, we show in figure 5 the distributions of the distances of Si, B, C and N atoms to the nearest Ar atom.

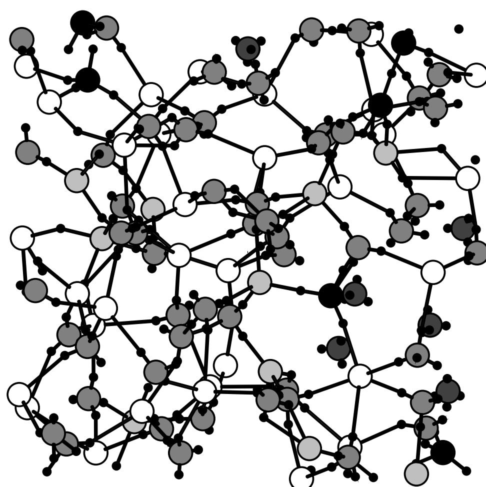

Figure 4. A snapshot from the end of a simulation of a structure of composition $Si_{32}B_{10}C_6N_{52}Ar_6$. Large black circles are C, medium grey are N, light grey are B, white are Si, and dark grey (isolated) circles correspond to Ar. The small black dots represent Wannier function centres (WFCs).

The distribution Si–Ar is more heavily weighted to short distances than are the distributions for the other atom types, suggesting the formation of Si-rich regions around implanted Ar atoms. The average composition of the part of the sample surrounding the implanted Ar atoms (within a radius of $\leqslant$3.6 Å) is $Si_{36}B_9C_6N_{49}$, while the average composition of the rest of the sample is $Si_{24}B_{13}C_6N_{57}$. Due to the previously shown preference for a homogenous structure in the sample without Ar, this difference can be considered significant.

An explanation of this phenomenon may be that the longer and more flexible Si bonds (in comparison to B, C and especially N bonds) allow the Ar induced cavities to be accommodated into the structure with minimal energy penalty including generated stress. The covalent radii of Si, B, C and N are 1.11, 0.82, 0.77 and 0.75 Å. In our structure the calculated average bond lengths (including bonds of all orders with all species) were 1.80 for Si-containing bonds and 1.51 for all other bonds. The Ar atoms sit in cavities with distances of at least 2.2 Å (lower bound of first peaks on figure 5) separating them from other atoms in the network. The longer bonds associated with Si allow Si-rich regions to contain natural cavities which are larger than in Si-poor regions. Such cavities allow the incorporation of Ar with minimum energy penalty. The flexibility of the long Si-containing bonds enables these bonds to deform to accommodate the Ar atoms with minimal generation of stress. This explains the experimental observation (figure 1) that compressive stress generated by implanted Ar is lowest in samples with highest Si content.

Deeper insight into the role of Ar in determining the structure of SiBCN materials can be gained by calculating selected statistics. Structural statistics comparing the $Si_{32}B_{10}C_6N_{52}$ and $Si_{32}B_{10}C_6N_{52}Ar_6$ samples, generated using cooling times of 500 fs (corresponding to the experimental $U_b = -500$ V), are shown in table 1.

Table 1 reveals several important features of the effects of Ar inclusion into the material. Si tends to accumulate in the vicinity of the Ar atoms. To show this, we use a statistic applying to the group of bonds surrounding Ar atoms. These are defined as those bonds which have a perpendicular distance of less than 2.5 Å to an Ar atom. Si is present in 96% of these bonds whereas it is only present in 73% and 75% of all bonds in the Ar-containing and Ar-free sample, respectively.

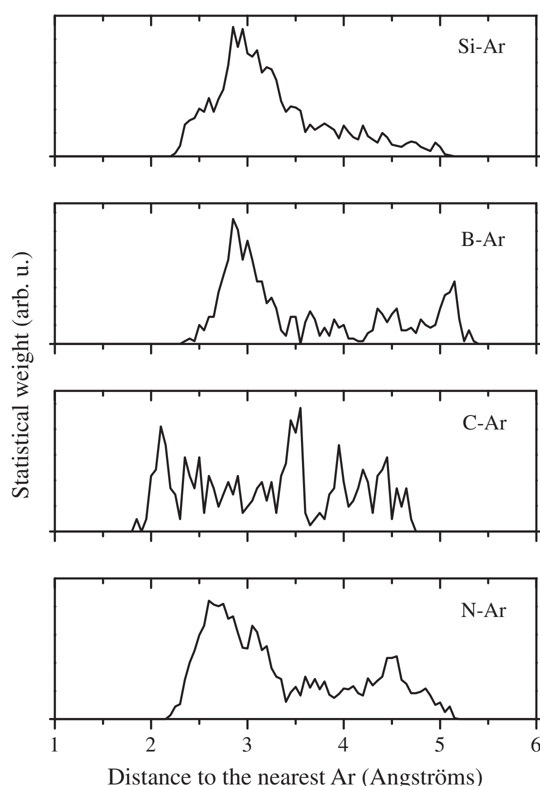

Figure 5. Distributions of distances of Si, B, C and N atoms to the nearest Ar atom in the sample $Si_{32}B_{10}C_6N_{52}Ar_6$. Data are summarized over all atoms of the respective kind and over 69 snapshots made during the 0.5 ps production run at the end of the liquid-quench simulation. In the Si–Ar distribution most of the distances are in the lower part of the range.

Table 1. Selected averaged statistics for simulated materials $Si_{32}B_{10}C_6N_{52}$ and $Si_{32}B_{10}C_6N_{52}Ar_6$. The Si content percentages, given in brackets, are for the subset of atoms and bonds in the 'vicinity' of Ar. Vicinity is defined for atoms as those which are closer than 3.6 Å to an Ar atom and bonds which have an Ar atom closer than 2.5 Å (perpendicular distance).

Quantity	SiBCN	SiBCNAr
Volume per atom (Å^3)	11.0	9.0
Si content	32%	32% (36%)
Si-containing bonds	75%	73% (96%)
Fraction of all B or C containing bonds which also include Si	9%	24% (66%)
Criterion 1 for segregation	43%	52%
Criterion 2 for segregation	9%	8%
Average length—all bonds (Å)	1.70	1.72
Average length—single BN (Å)	1.51	1.55
Average length—single CN (Å)	1.41	1.46
Number of rings	9.0	18.6
Average ring size	5.8	6.0

The presence of Ar induces a major shift in the bonding preferences of all atom types. To show this we use the statistic shown in row 4 of table 1. B, C and Si tend to form bonds

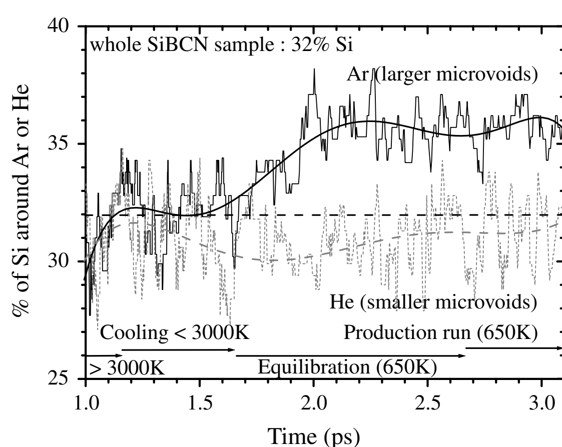

Figure 6. The development of the segregation of Si around implanted Ar/He atoms during the liquid-quench simulation of $Si_{32}B_{10}C_6N_{52}Ar_6$ and $Si_{32}B_{10}C_6N_{52}He_6$ structures. The y-axis shows the Si content percentages in the subset of atoms in the vicinity of Ar or He. Atoms in the vicinity are defined as those which are closer than 3.6 Å to an Ar or 3.2 Å to a He atom, respectively. The x-axis shows the time from start of the liquid-quench simulation. The averaged stable percentage of Si around implanted Ar/He atoms is close to the Si content in whole SiBCN sample for He, while it is significantly higher for Ar.

with N in the absence of Ar, B exclusively whereas C and Si preferentially. This effect has also been noted in our experimental observations [15]. In the simulated Ar-containing sample the tendency for B and C to bond with Si is greatly increased. In the Ar-free sample, only 9% of all bonds containing B or C contain Si, whereas in the Ar-containing sample 24% of all bonds containing B or C contain Si. In the group of bonds surrounding Ar atoms, the effect is even more pronounced with 66% of bonds containing B or C containing Si. These changes in bonding preference with the introduction of Ar are reflected in the increase in Criterion 1 as shown in row 5 of table 1.

Although the Ar-containing sample is more compressed (smaller volume per atom as shown in row 1 of table 1), it is remarkable that the averaged bond length is higher (row 7) than that for the Ar-free sample. This is not only due to the higher total percentage of longer Si-containing bonds, but also to the longer bonds of certain types (single BN, single CN) prevailing in the part of the sample far from the Ar atoms (rows 8 and 9).

Adding Ar to the sample also has a major impact on the topology of the network as revealed by the ring statistics. In the last two rows of table 1, we see that the number of rings is doubled after addition of Ar. The numbers of the rings were calculated using the algorithm of Franzblau [34].

Figures 6 and 7 show the effect of temperature on the segregation of Si around Ar atoms. Segregation is not stable in the molten state and is expected to occur below some temperature limit. The development of the percentage of Si around (up to 3.6 Å) Ar atoms during the liquid-quench simulation of the sample $Si_{32}B_{10}C_6N_{52}Ar_6$ is shown in figure 6. The trendline shows that this quantity starts to increase in the equilibration phase at the end of the cooling and increases during the equilibration until a maximum has been reached. The maximum exists because diffusion is limited once the solid has formed.

Figure 6 also shows the same statistic in which the Ar was replaced with He. The same atomic density and cooling time have been used for this simulation. The first minima of the pair correlation functions in which one of the atoms is He are around 1.9 Å in comparison with

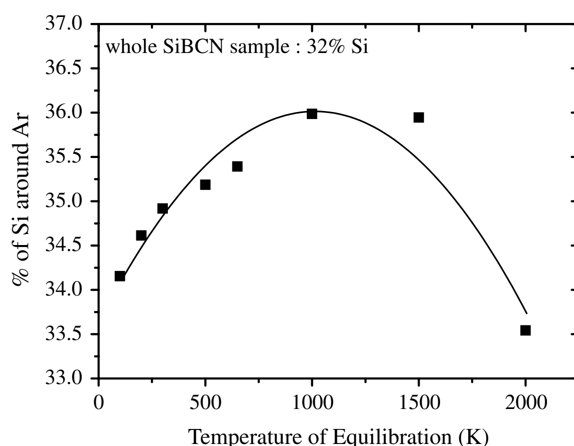

Figure 7. Segregation of Si around implanted Ar atoms in samples of composition $Si_{32}B_{10}C_6N_{52}Ar_6$ equilibrated at various temperatures. The vertical axis refers to the percentage of Si atoms in the group of Si, B, C and N atoms that lie in the vicinity of an Ar atom. Atoms in the vicinity are defined as those which are closer than 3.6 Å to an Ar. The data are averaged over the stable period 0.5–1 ps from the start of equilibration. The percentage of Si around Ar reaches a maximum for equilibration temperatures in the range 1000–1500 K.

2.2 Å for the Ar case. It suggests that the envelopes around smaller cavities containing He can be formed from all bond types rather than only from the long Si-containing bonds as in the Ar-containing structure. Thus, there is not any observable segregation of Si around implanted He atoms.

In order to examine the effect of equilibration temperature on segregation of Si around Ar more closely, we performed a series of constant temperature 1 ps MD runs at temperatures between 100 and 2000 K. These simulations used the (nearly homogenous) starting structure of the previous equilibration at 650 K. The velocities were scaled in accordance with the new temperature. For all temperatures, the percentage of Si around Ar atoms increased during the first 0.5 ps of equilibration while the mean value was stable during the second 0.5 ps. Figure 7 shows averaged stable values of percentages of Si around Ar for all simulated equilibration temperatures. This figure also shows that for equilibration temperatures between 100 and 1000 K, the segregation of Si around Ar increases with increasing temperature. We attribute this to increasing temperature-dependent diffusion coefficients. At higher temperatures, the kinetic energies of atoms may be comparable or larger than the energy penalty associated with having the Ar cavities surrounded also by short and inflexible non-Si-containing bonds. This leads to a reduction in the degree of Si segregation around the Ar. These results lead us to predict that Si should relax the compressive stress generated in films deposited using Ar sputtering more effectively at higher deposition temperatures provided that the temperature is below 1000 K.

4. Conclusion

We report experimental results showing the correlation of stress in SiBCN films prepared by sputtering in Ar with the content of Ar in the film. The correlation decreases steadily with increasing Si content.

We investigated using liquid-quench simulations the origin of the ability of Si to reduce the stress generated in these films by Ar. The simulations show that SiBCN has a preference for

a completely homogenous structure in the absence of Ar. When Ar atoms were included in the simulation, we observed the segregation of a Si-rich regions around them. We propose that the driving force for the segregation is the energy advantage gained by surrounding Ar atoms with longer and more flexible Si-containing bonds. This explains the ability of Si to inhibit the extra stress, otherwise generated by implanted Ar in SiBCN materials with zero or low Si content.

The incorporation of Ar in the simulations caused major changes in the bonding preferences of all the atoms in the network. For example, all atoms showed a preference for bonding to N in the absence of Ar, whereas they showed a general increase in bonding to Si when Ar is present.

Based on the simulations, we make the prediction that the effectiveness of Si to relieve stress in SiBCN films sputtered in Ar will increase with deposition temperature up to ≈1000 K.

Acknowledgments

This work was supported by the Australian Partnership for Advanced Computing (APAC), the Australian Centre for Advanced Computing and Communications (AC3) and the Ministry of Education of the Czech Republic through project No. MSM 4977751302.

References

[1] Ramakrishnan P A, Wang Y T, Balzar D, An L, Haluschka C, Riedel R and Hermann A M 2001 *Appl. Phys. Lett.* **78** 3076
[2] Baufeld B, Gu H, Bill J, Wakai F and Aldinger F 1999 *J. Eur. Ceram. Soc.* **19** 2797
[3] Jungermann H and Jansen M 1999 *Mater. Res. Innovat.* **2** 200
[4] Riedel R, Kienzle A, Dressler W, Ruwisch L, Bill J and Aldinger F 1996 *Nature* **386** 796
[5] Schmidt S, Borchardt G, Weber S, Scherrer H, Baumann H, Müller A and Bill J 2002 *J. Non-Cryst. Solids* **298** 232
[6] Müller A, Gerstel P, Weinmann M, Bill J and Aldinger F 2000 *J. Eur. Ceram. Soc.* **20** 2655
[7] Müller A, Gerstel P, Weinmann M, Bill J and Aldinger F 2001 *J. Eur. Ceram. Soc.* **21** 2171
[8] Müller A, Zern A, Gerstel P, Bill J and Aldinger F 2002 *J. Eur. Ceram. Soc.* **22** 1631
[9] Lu L, Song Y C and Feng C X 1998 *J. Mater. Sci. Lett.* **17** 599
[10] Butchereit E and Nickel K G 2001 *J. Am. Ceram. Soc.* **84** 2184
[11] Riedel R, Ruwisch L M, An L and Raj R 1998 *J. Am. Ceram. Soc.* **81** 3341
[12] Hegemann D, Riedel R and Oehr C 1999 *Chem. Vapor Depos.* **5** 61
[13] Hegemann D, Oehr C and Riedel R 1999 *Proc. 14th Int. Symp. Plasma Chemistry (Prague)* vol 3, ed M Hrabovsky *et al* p 1573
[14] Rooke M A and Sherwood P M A 1997 *Chem. Mater.* **9** 285
[15] Vlcek J, Potocky S, Cizek J, Houska J, Kormunda M, Zeman P, Perina V, Zemek J, Setsuhara Y and Kumagai M 2005 *J. Vac. Sci. Technol.* A **23** 1513
[16] Sproul W D *et al* (ed) 1986 *Physics and Chemistry of Protective Coatings* (New York: American Institute of Physics) pp 56–8
[17] Davis C A 1993 *Thin Solid Films* **226** 30
[18] Ulrich S, Theel T, Schwan J and Ehrhardt H 1997 *Surf. Coat. Technol.* **97** 45
[19] CPMD, Copyright IBM Corp. 1990–2005, Copyright MPI für Festkörperförschung Stuttgart 1997–2005
[20] Becke A D 1988 *Phys. Rev.* A **38** 3098
[21] Lee C, Yang W and Parr R G 1988 *Phys. Rev.* B **37** 785
[22] Goedecker S, Teter M and Hutter J 1996 *Phys. Rev.* B **54** 1703
[23] Troullier N and Martins J L 1991 *Phys. Rev.* B **43** 1993
[24] Houska J, Bilek M M M, Warschkow O, McKenzie D R and Vlcek J 2005 *Phys. Rev.* B **72** 054204
[25] Marks N A 1997 *Phys. Rev.* B **56** 2441
[26] Marks N A, Cooper N C, McKenzie D R, McCulloch D G, Bath P and Russo S P 2002 *Phys. Rev.* B **65** 75411
[27] McCulloch D G, McKenzie D R and Goringe C M 2000 *Phys. Rev.* B **61** 2349
[28] Bilek M M M, McKenzie D R, McCulloch D G and Goringe C M 2000 *Phys. Rev.* B **62** 3071
[29] Merchant A R, McKenzie D R and McCulloch D G 2001 *Phys. Rev.* B **65** 24208

[30] McCulloch D G, McKenzie D R and Goringe C M 2000 *J. Appl. Phys.* **88** 5028
[31] Fitzhenry P, Bilek M M M, Marks N A, Cooper N C and McKenzie D R 2003 *J. Phys.: Condens. Matter* **15** 165
[32] Houska J *et al* 2005 *Mol. Simul.* submitted
[33] Gunnars J and Wiklund U 2002 *Mater. Sci. Eng.* A **336** 7
[34] Franzblau D S 1991 *Phys. Rev.* B **44** 4925